



Effects of heavy rare-earth addition on glass-forming ability, thermal, magnetic, and mechanical properties of Fe-RE-B-Nb (RE = Dy, Ho, Er or Tm) bulk metallic glass



Feng Hu^a, Chenchen Yuan^a, Qiang Luo^a, Weiming Yang^b, Baolong Shen^{a,b,*}

^a School of Materials Science and Engineering, Jiangsu Key Laboratory for Advanced Metallic Materials, Southeast University, Nanjing 211189, China

^b Institute of Massive Amorphous Metal Science, China University of Mining and Technology, Xuzhou 221116, China

ARTICLE INFO

Keywords:

Fe-based BMGs
Glass-forming ability
Electronic structure
Soft magnetic properties

ABSTRACT

With the aim of investigating how the species of doped rare-earth (RE) elements affect the glass-forming ability (GFA), 5 at. % RE elements were added in Fe₇₁Nb₆B₂₃ alloy to substitute Fe. Compared with the Fe₆₆RE₅Nb₆B₂₃ (RE = Ho or Dy), Fe₆₆RE₅Nb₆B₂₃ (RE = Er or Tm) possesses an extra competitive Fe₃B crystallization phase, which leads to a better GFA by stabilizing the liquid phase structure. Moreover, Fe₆₆Tm₅Nb₆B₂₃ shows the lowest density of states near the Fermi level among four alloys, which contributes to its best GFA. The influences of RE addition on the thermal, magnetic, and mechanical behaviors were also investigated. With increasing atomic number of RE elements from Dy to Tm, the saturation magnetic flux density increases obviously accompanied by the improved flowability in the supercooled liquid region, which makes Fe₆₆Tm₅Nb₆B₂₃ as a potential functional soft-magnetic material for thermoplastic machining.

1. Introduction

Fe-based bulk metallic glasses (BMGs) are promising candidates as advanced structural/functional materials due to their excellent soft magnetic performances, unique mechanical properties, corrosion resistance and so on [1–4]. Among Fe-based BMGs, Fe₇₁Nb₆B₂₃ is the strongest with outstanding fracture strength (σ_f) of about 4.85 GPa [5]. However, the low glass-forming ability (GFA) may restrain its potential industrial applications. The technology of microalloying has been widely applied in metallurgy field and played significant roles in the GFA, thermal stability or crystallization behavior of BMGs [6–8]. Through this method, we found that the thermal stability of supercooled liquid and GFA in FeNbB glassy alloy were enhanced appreciably by doping minor rare-earth (RE) elements [9,10]. Based on our previous work, it can be seen that the GFA of some Fe-based glassy alloys is not only affected by the content but also by the species of doped RE elements. Ab initio molecular dynamics simulation also shows that the different RE elements have a strong impact on the configuration of Fe-based alloy liquid, which results in a different GFA [11]. Besides of GFA, the local atomic structure, bonding environment, and mechanical properties are also influenced by minor RE elements addition [12–15]. Therefore, we have a great interest in how the RE elements affect us designing Fe-based BMGs on these aspects.

It has been reported that 5 at. % Ho or Er addition to Fe₇₁Nb₆B₂₃ is optimum for improving the GFA and supercooled liquid region (SCLR) [9,10]. Moreover, doping 5 at. % Er elements can effectively tune the magnetic transition (T_C) near room temperature in FeErNbB alloy system. Thus, with the aim of better understanding how the GFA, thermal, magnetic, and mechanical properties of Fe₇₁Nb₆B₂₃ BMG are affected by doping different RE elements, 5 at.% Dy, Ho, Er, and Tm elements were added to Fe₇₁Nb₆B₂₃ alloy to substitute Fe, respectively. We found that the GFA of Fe₆₆RE₅Nb₆B₂₃ (RE = Dy, Ho, Er or Tm) glassy alloy has a strong correlation with primary crystallization phases and electronic structure. Doping different heavy RE elements precipitates into distinct crystallization phases and causes the disparity of density of states near the Fermi level $N(E_F)$, which gives rise to different GFA in this alloy system. In addition, the investigations based on thermal and magnetic properties of these glassy alloys show that both the GFA and the saturation magnetic flux density (B_s) increase with an increasing atomic number of RE elements. Despite of the decrease of σ_f at room temperature with the addition of RE elements, the wide SCLR and the softened behavior in SCLR make Fe₆₆RE₅Nb₆B₂₃ as good candidates for thermal machining in the SCLR.

* Corresponding author at: School of Materials Science and Engineering, Southeast University, Nanjing 211189, China.

E-mail address: blshen@seu.edu.cn (B. Shen).

<https://doi.org/10.1016/j.jnoncrysol.2019.119681>

Received 22 July 2019; Received in revised form 2 September 2019; Accepted 6 September 2019

0022-3093/© 2019 Elsevier B.V. All rights reserved.

2. Experimental

$\text{Fe}_{66}\text{RE}_5\text{Nb}_6\text{B}_{23}$ quaternary alloy ingots (RE = Dy, Ho, Er or Tm) were prepared in a copper crucible. The ribbon samples were produced by a single roller melt-spinning method. Glassy rods with diameters up to 4.5 mm were made by copper mold casting. The thermal behaviors were measured with differential scanning calorimetry (DSC, NETZSCH 404 F3) using Al_2O_3 crucible. Samples were crystallized by annealing at a pressure of 2×10^{-3} Pa for 600 s at 1043 K in the annealing furnace and crystallization phases were examined by X-ray diffraction (XRD, Bruker D8 Discover diffractometer). Transverse cross-section of the as-cast glassy alloy rods was examined by scanning electron microscopy (SEM, FEI Sirion 200). X-ray photoelectron spectrometer (XPS, ESCALAB 250XI) was employed to measure electronic structures with Al $K\alpha$ X-ray source. Prior to XPS measurements, the sample surfaces were cleaned via argon ion sputtering for 500 s. The thermal dilatation (DIL) measurement was carried out by using the TMA (NETZSCH, 402C) with a dimension of 1.5 mm. Compressive fracture strength (σ_f) was measured using glassy rods with a diameter of 1 mm and a length of 2 mm by the testing machine (CMT 4503) with a compressive strain rate of $5 \times 10^{-4} \text{ s}^{-1}$. Vickers hardness (H_v) was measured by a hardness tester (FM-700) under a load of 9.8 N. The B_s versus field ($B-H$) of the ribbons was measured by vibrating sample magnetometer (VSM, Lake Shore 7410). Coercivity (H_c) was measured by a DC $B-H$ loop tracer (RIKEN BHS-40). To estimate the uncertainty of each measurement of thermal, magnetic and mechanical properties, at least four measurements were conducted. The thermal parameters, magnetic parameters (B_s , H_c), and mechanical parameters (H_v , σ_f) were determined by averaging the measured values.

3. Results and discussion

For the purpose of evaluating the GFA through an experimental method, BMG rods with different diameters were fabricated for the RE (RE = Dy, Ho, Er or Tm) doped alloys $\text{Fe}_{66}\text{RE}_5\text{Nb}_6\text{B}_{23}$. Fig. 1 shows the XRD patterns of the $\text{Fe}_{66}\text{RE}_5\text{Nb}_6\text{B}_{23}$ cast rods. They all show typical broad peak without sharp crystallization peak. Fig. 2(a)–(d) shows cross-sectional morphologies of the as-cast $\text{Fe}_{66}\text{RE}_5\text{Nb}_6\text{B}_{23}$ (RE = Dy, Ho, Er, and Tm) rods with critical diameters. No distinct crystalline grains can be seen in the cross-section by both low power and high power SEM observation, which is consistent with the XRD results. The critical diameters (D_c) of the BMG rods are 2, 3, 4, and 4.5 mm respectively for the $\text{Fe}_{66}\text{RE}_5\text{Nb}_6\text{B}_{23}$ (RE = Dy, Ho, Er or Tm) glassy alloys. However, the atomic mismatch and the mixing enthalpy between RE element and the other three elements are almost the same [16]. Thus, the increase in D_c as a function of an ordinal number of the heavy RE element should be taken into further consideration.

The DSC traces of the $\text{Fe}_{66}\text{RE}_5\text{Nb}_6\text{B}_{23}$ (RE = Dy, Ho, Er or Tm)

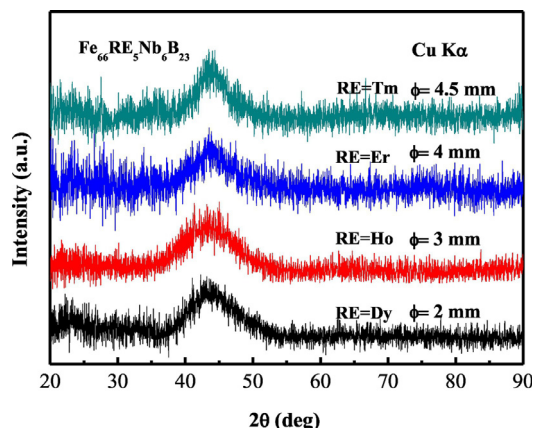


Fig. 1. XRD patterns of the $\text{Fe}_{66}\text{RE}_5\text{Nb}_6\text{B}_{23}$ (RE = Dy, Ho, Er or Tm) glassy rods.

glassy ribbons in the temperature range from 600 to 1220 K are shown in Fig. 3. They all exhibit an obvious glass transition and a wide SCLR. The glass transition temperature (T_g) and the onset temperature of crystallization (T_x) show no significant change by doping different RE elements. The SCLR ($\Delta T_x = T_x - T_g$) (about 90 K) is extended by adding a minor RE elements as compared with the initial composition of $\text{Fe}_{71}\text{Nb}_6\text{B}_{23}$ ($\Delta T_x = 39 \text{ K}$) [7]. It indicates that the minor RE element addition is effective for the extension of SCLR in this alloy system. The abnormal exothermic peak marked as P_0 (corresponding to T_{in}) is observed in the SCLR for these alloys, and this phenomenon has been well discussed in our recent work [10]. In addition, they exhibit distinct crystallization behavior of DSC curve as shown in Fig. 3. It can be found that it appears a small divisive peak (marked as P_1) before the main exothermic peak (marked as P_2) upon Dy addition. While with Ho addition, P_1 becomes a shoulder-like peak (marked as P_{sho1}). For the alloy containing Er element, the shoulder-like peak (marked as P_{sho2}) emerges on the right of the P_2 peak, and when Tm element was doped, it forms a new peak marked as P_3 . Anyway, the addition of different RE elements causes totally different crystallization behaviors, this may have a relationship with the variation in GFA.

For further studying the relationship between the GFA and crystallization behaviors, and figuring out how crystallization behaviors of this alloy system are affected by the RE elements, $\text{Fe}_{66}\text{RE}_5\text{Nb}_6\text{B}_{23}$ were isothermally annealed in an annealing furnace. Fig. 4 shows XRD patterns of the $\text{Fe}_{66}\text{RE}_5\text{Nb}_6\text{B}_{23}$ glassy ribbons annealed at 1043 K for 600 s. It can be seen that Dy- and Ho- containing glassy samples show the precipitation phases of Fe_{23}B_6 and $\text{RE}_2\text{Fe}_{14}\text{B}$, however, the precipitation phases are changed into Fe_{23}B_6 , $\text{RE}_2\text{Fe}_{14}\text{B}$, and Fe_3B with Er and Tm addition. Besides, the peak of $\text{RE}_2\text{Fe}_{14}\text{B}$ at $2\theta = 42.6^\circ$ becomes gradually dominant compared with the appearance of the peak for Fe_{23}B_6 at $2\theta = 43.6^\circ$ with increasing RE atomic number. Thus, the P_1 and P_2 peaks should correspond to the precipitation of $\text{RE}_2\text{Fe}_{14}\text{B}$ and Fe_{23}B_6 phases respectively in the DSC curve for Dy-containing BMG. Due to the increasing amount of precipitated $\text{Ho}_2\text{Fe}_{14}\text{B}$ phase, the P_1 peak becomes a shoulder-like peak (marked as P_{sho1}) with Ho addition. The P_{sho2} peak should be caused by the precipitation of Fe_3B phase for the $\text{Fe}_{66}\text{Er}_6\text{Nb}_6\text{B}_{23}$ ribbon, and P_{sho2} peak becomes stronger to form a P_3 peak for Tm-containing alloy. It has been reported that the primary crystallization phase for the $\text{Fe}_{71}\text{Nb}_6\text{B}_{23}$ sample is the metastable Fe_{23}B_6 phase [5,7], and the new formed competitive $\text{RE}_2\text{Fe}_{14}\text{B}$ phase makes atomic diffusion of the whole sample more difficult, leading to the increase of GFA in $\text{Fe}_{66}\text{RE}_5\text{Nb}_6\text{B}_{23}$ glassy alloys [10]. Besides, due to the fact that the amount of $\text{Ho}_2\text{Fe}_{14}\text{B}$ precipitated phase is more than that of $\text{Dy}_2\text{Fe}_{14}\text{B}$ precipitated phase, it causes a higher competition between $\text{RE}_2\text{Fe}_{14}\text{B}$ and Fe_{23}B_6 phases, which might response for the higher GFA of $\text{Fe}_{66}\text{Ho}_5\text{Nb}_6\text{B}_{23}$ than that of $\text{Fe}_{66}\text{Dy}_5\text{Nb}_6\text{B}_{23}$. Because that $\text{Fe}_{66}\text{RE}_5\text{Nb}_6\text{B}_{23}$ (RE = Er or Tm) owns an extra Fe_3B precipitated phase, it exhibits a multiphase crystallization behavior. Such competition of multiphases is beneficial for the stabilization of the liquid phases, which may improve the GFA of RE-added $\text{Fe}_{66}\text{RE}_5\text{Nb}_6\text{B}_{23}$ (RE = Er or Tm) alloy systems.

The GFA is not only affected by atomic stacking but also by electronic structure [17–19]. With the aim of exploring the electronic structure, the core-level spectra of participating elements in the $\text{Fe}_{66}\text{RE}_5\text{Nb}_6\text{B}_{23}$ glassy alloys were measured, as seen in Fig. 5. The Fe 2p, B 1s, and Nb 3d level spectra derived from the $\text{Fe}_{66}\text{RE}_5\text{Nb}_6\text{B}_{23}$ ribbons are shown in Fig. 5(a), (b), and (c). The binding energy (BE) position of the Fe 2p_{3/2} and B 1s changes very small (lower than 0.1 eV). The BE position of the Fe 2p_{3/2} has same tendency with the observation of $(\text{Fe}_{0.71}\text{RE}_{0.05}\text{B}_{0.24})_9\text{Nb}_4$ (RE = Gd, Tb, Ho, Er or Tm) glassy alloys [18], which may indicate the change of electronic density of state. There is no significant change in Nb 3d_{5/2} BE (about 202.90 eV), probably because that the enthalpy of mixing between Nb and RE is positive and high, which may cause phase separation in this alloy system [20]. Meanwhile, since Er and Tm are more likely to form $\text{RE}_2\text{Fe}_{14}\text{B}$ phase, it causes the Nb element is more likely to facilitate the

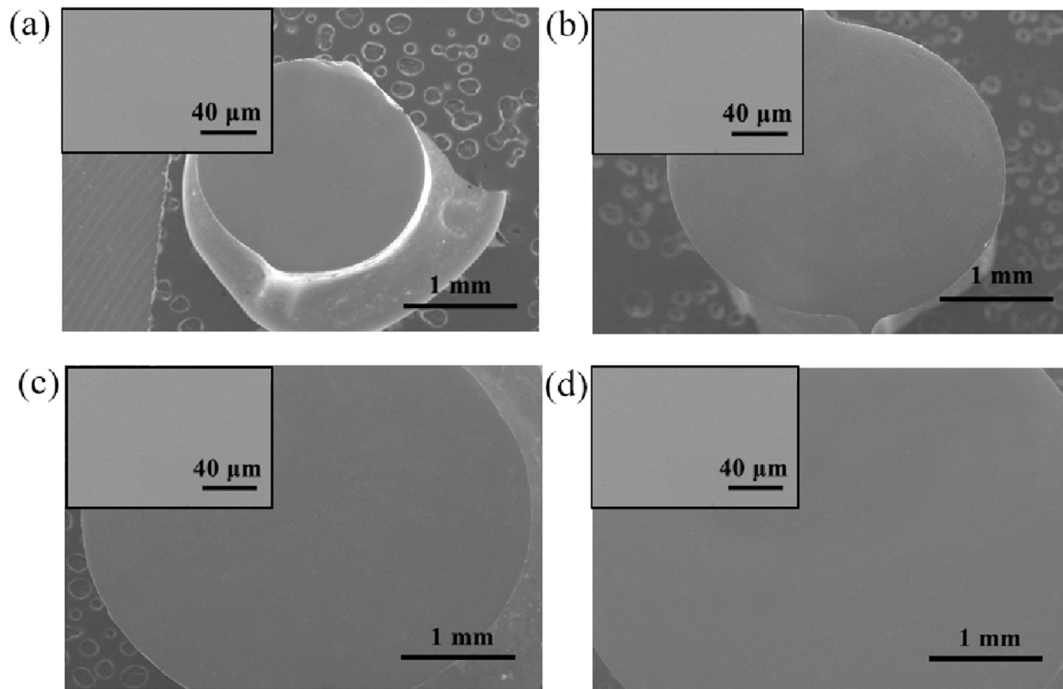


Fig. 2. SEM images of the transverse cross-section of the as-cast $\text{Fe}_{66}\text{RE}_5\text{Nb}_6\text{B}_{23}$ glassy rods with critical diameters: (a) $\text{Fe}_{66}\text{Dy}_5\text{Nb}_6\text{B}_{23}$, (b) $\text{Fe}_{66}\text{Ho}_5\text{Nb}_6\text{B}_{23}$, (c) $\text{Fe}_{66}\text{Er}_5\text{Nb}_6\text{B}_{23}$, and (d) $\text{Fe}_{66}\text{Tm}_5\text{Nb}_6\text{B}_{23}$. The insets are the corresponding high energy SEM images.

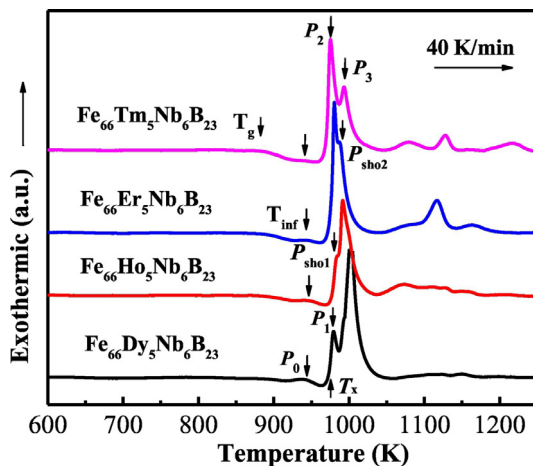


Fig. 3. DSC curves of the melt-spun $\text{Fe}_{66}\text{RE}_5\text{Nb}_6\text{B}_{23}$ (RE = Dy, Ho, Er or Tm) glassy ribbons.

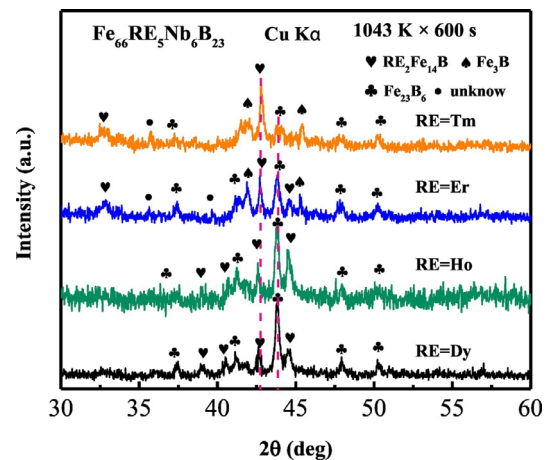


Fig. 4. XRD patterns of $\text{Fe}_{66}\text{RE}_5\text{Nb}_6\text{B}_{23}$ (RE = Dy, Ho, Er or Tm) ribbons annealed at 1043 K for 600 s.

formation of crystallization phases of Fe_{23}B_6 and Fe_3B [21,22]. Fig. 5(d) shows the valence band structure of $\text{Fe}_{66}\text{RE}_5\text{Nb}_6\text{B}_{23}$ (RE = Dy, Ho, Er or Tm). The spectra are marked differently from that of pure Fe in the region from 6 to 10 eV. It is attributed to the overlapped B 2s and RE 4f state that leads to the enhancement of RE-B bonds [18]. Based on the nearly-free-electron model [23], the better GFA the alloy has, the lower the density of states near the Fermi level $N(E_F)$ is [17,23]. As shown in inset Fig. 5(d), it can be found that $N(E_F)$ decreases when Dy was substituted by Tm element, therefore, Tm doped alloy owns the most stable state and the best GFA among this alloy system [17].

As discussed above, the atomic stacking can be affected by the heavy RE elements alloying, DIL measurement was carried out by using the TMA to measure the changes of expansion coefficients and thermal behaviors in this alloy system. Fig. 6 shows the DIL traces of $\text{Fe}_{66}\text{RE}_5\text{Nb}_6\text{B}_{23}$ (RE = Dy, Ho, Er, or Tm) glassy alloys. It can be found that the glassy specimen expands linearly with rising temperature, this may be caused by enhanced the atomic thermal vibration behaviors

[24]. Doping different heavy RE elements in $\text{Fe}_{71}\text{Nb}_6\text{B}_{23}$ alloy show a similar linear expansion process and the average coefficient of the linear expansion marked as α_L is all about $7 \times 10^{-6} \text{K}^{-1}$. It indicates that the addition of RE elements may influence the atomic packing, however such effect before T_g is very small and can be neglected. A rapid contraction arises when the samples are heated to SCLR. The softness denoted as $(\Delta L/L_0)_{s-\max}$ of SCLR usually has a close correlation with the viscosity that affected by heavy RE elements [25], as shown Fig. 6. Based on the rheological model that describes viscosity and iso-configuration shear modulus G [26], Hu Q. et al. considered that the softness relates to $\Delta G = G(\text{Fe}_{71}\text{Nb}_6\text{B}_{23}) - G(\text{RE})$ [25]. The G of $\text{Fe}_{71}\text{Nb}_6\text{B}_{23}$ BMG reported by Park J. is 73.4 GPa [27], and for the pure Dy, Ho, Er, Tm, G_s are 25, 26, 28, and 31 GPa [28], respectively. The ΔG can be obtained using the formula $\Delta G = G(\text{Fe}_{71}\text{Nb}_6\text{B}_{23}) - G(\text{RE})$. Its relation with softness is plotted in the inset of Fig. 6. It can be found that the softness shows a good linear negative correlation with ΔG in $\text{Fe}_{66}\text{RE}_5\text{Nb}_6\text{B}_{23}$ alloy system. Smaller ΔG corresponds to a better

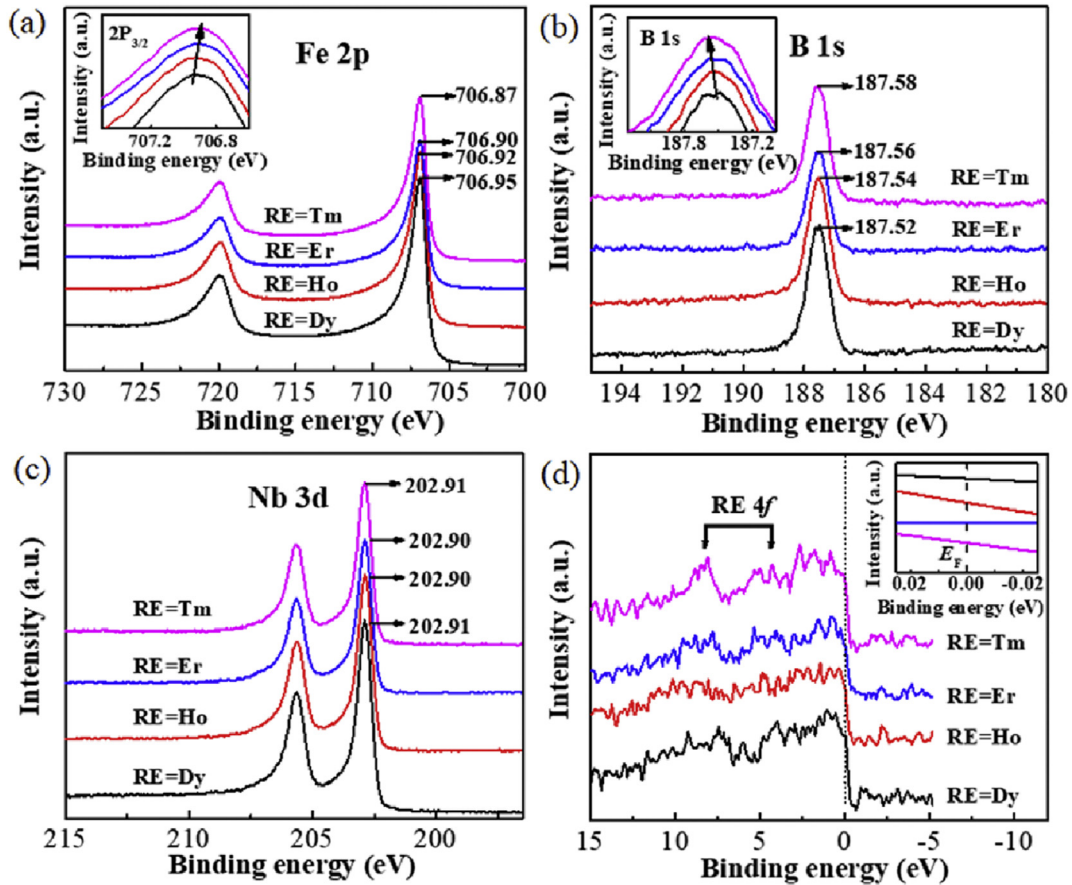


Fig. 5. XPS spectra of the $Fe_{66}RE_5Nb_6B_{23}$ (RE = Dy, Ho, Er or Tm) glassy ribbons: (a) core-level spectra of Fe 2p, (b) core-level spectra of B 1s, (c) core-level spectra of Nb 3d, and (d) valence band spectra.

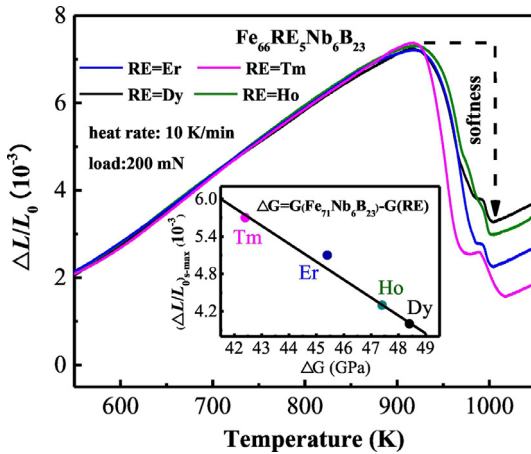


Fig. 6. DIL traces of $Fe_{66}RE_5Nb_6B_{23}$ (RE = Dy, Ho, Er or Tm) glassy alloys, the inset shows the correlation between $(\Delta L/L_0)_{s-max}$ and ΔG .

flowability in SCLR [25], therefore, $Fe_{66}Tm_5Nb_6B_{23}$ alloy may be more suitable for thermoplastic machining in the SCLR among these four alloys.

The soft magnetic properties of $Fe_{66}RE_5Nb_6B_{23}$ (RE = Dy, Ho, Er or Tm) glassy alloys were also investigated. Fig. 7 displays the $B-H$ hysteresis curves measured by VSM. It can be seen that in $B-H$ loop tracer, the rapidly saturated magnetization indicates the excellent soft magnetic properties. It ascribes to the homogeneous structure of this metallic glass alloy without grain boundary to nail the domain wall. The B_s increases gradually from 0.46 to 0.58 T with doping RE element from

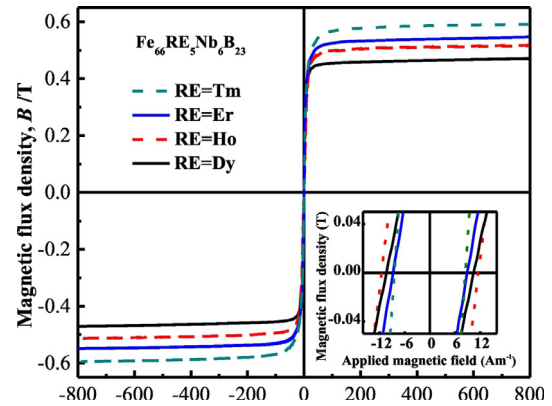


Fig. 7. $B-H$ hysteresis curves of the annealed melt-spun $Fe_{66}RE_5Nb_6B_{23}$ (RE = Dy, Ho, Er or Tm) glassy ribbons measured by VSM. The insert is the enlarged $B-H$ loop tracer.

Dy to Tm. It is known that the electron in the 3d shell of Fe atom couples is antiferromagnetic with the electron in the 4f shell of RE atom, the smaller magnetic moment of RE element is, and the higher B_s of this glassy alloy shows [29]. The magnetic moments of Dy, Ho, Er, and Tm are 10.6, 10.6, 9.6, and 7.6 μ_B , respectively. Therefore, Tm-containing sample has the highest B_s among these four glassy alloys. On the other hand, B element has a negative effect on the ferromagnetism of the FeNbB alloy system in B-rich compositions [30]. The overlapping of B 2s and RE 4f state discussed in core-level spectra correspond to the strong RE-B bonds near the Fermi level [18]. According to the near neighbor model of B-centered atom, the increase of interaction between

RE and B atoms may weaken the interaction between atom B and Fe atoms, which may reduce the negative effect of B on the ferromagnetism of Fe-based alloys and response for the small change of BE position of the B 1s as shown in Fig. 5(b). Thus, minor RE addition may be beneficial for high magnetic performances in some case. The H_c value is highly affected by magnetic anisotropy and sample quality [18,31]. It is difficult to control the same size and quality of the prepared ribbons because the samples are very brittle after doping RE elements. Thus, no gradual regularity of H_c is observed in this alloy system. However, due to the reason that the exchange energy of Tm–Fe is lower than the other three RE–Fe atomic pairs, it may have the smallest magnetic anisotropy constant K [18], which results in the lowest H_c value among these four alloys. On the other hand, because that the saturation magnetostriction (λ_s) can be enhanced by doping RE element in Fe-based glassy alloy [32], and it has a positive correlation with H_c^σ [33],

$$H_c^\sigma \approx |\sigma \lambda_s| / |M_s| \quad (1)$$

where M_s is the saturation magnetization and H_c^σ coercivity which originates from the magnetoelastic coupling. Therefore, the contribution of H_c^σ and magnetic anisotropy to the total H_c of $\text{Fe}_{66}\text{RE}_5\text{Nb}_6\text{B}_{23}$ (RE = Dy, Ho, Er or Tm) is larger than that of $\text{Fe}_{71}\text{Nb}_6\text{B}_{23}$ ($H_c = 3.9 \text{ A/m}$).

Except for excellent GFA and soft magnetic properties, $\text{Fe}_{66}\text{RE}_5\text{Nb}_6\text{B}_{23}$ (RE = Dy, Ho, Er or Tm) also shows superhigh σ_f and Vickers hardness which are summarized in Table 1. The stress-strain curves show a downtrend in Fig. 8. By doping 5 at. % RE elements, the discrete nature of σ_f becomes much more obvious, especially for the composition containing Er and Tm elements. It has been proposed that the fracture strength and toughness of BMG can be manipulated by the degree of bonding hybridization [34,35], i.e. the density of state at the Fermi level. As shown in Fig. 5(d), the lowest $N(E_F)$ of Tm-containing glassy alloy indicates a weaker atomic bonding than that of other three RE elements containing system [35], which causes the decrease of both fracture strength and Vickers hardness. Meanwhile, as reported in the work of Liu [36] and Li [37] et al., the minor RE alloying may cause the high flaw sensitivity and porosity, which easily causes a premature fracture before the intrinsic strength of materials. This might be another reason that decreases the σ_f of Er- or Tm-containing sample. However, although σ_f of Tm-containing sample is lower than that of Dy- and Ho-containing samples, it still exceeds σ_f of many metal materials.

In our recent work, thermoplastic deformation of $\text{Fe}_{66}\text{Ho}_5\text{Nb}_6\text{B}_{23}$ glassy alloy has been investigated [10]. It was found that RE-containing Fe-based BMGs own a wide SCLR, which can be used for thermoplastic processing at the temperature above room temperature. The present studied RE-added $\text{Fe}_{66}\text{RE}_5\text{Nb}_6\text{B}_{23}$ BMGs also exhibit a wide SCLR of about 90 K, which make them be suitable for thermoplastic processing in the SCLR as well. Based on the further analysis of the DIL measurement and magnetic properties, it is proposed that $\text{Fe}_{66}\text{Tm}_5\text{Nb}_6\text{B}_{23}$ alloys with good flowability and soft magnetic property can be as a promising thermoplastic-machining functional material for industrial applications in the near future.

Based on the above experimental results, heavy RE elements addition on $\text{Fe}_{71}\text{Nb}_6\text{B}_{23}$ can improve comprehensive performance

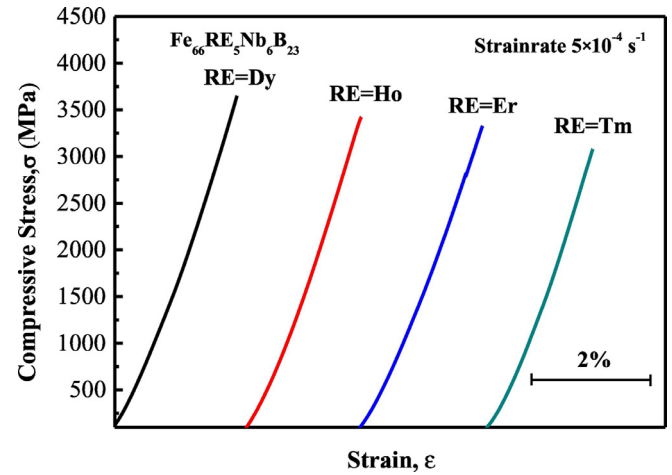


Fig. 8. The compressive stress-strain curves of 1 mm $\text{Fe}_{66}\text{RE}_5\text{Nb}_6\text{B}_{23}$ (RE = Dy, Ho, Er or Tm) as-cast rods at room temperature.

effectively. The radius of heavy RE element decreases and the electron number of 4f electronic shell increases as the atomic number increases, which leads to the changes of atomic stacking and electronic structures of FeRENbB alloy system. The XPS result shows that $N(E_F)$ decreases when Dy was substituted by Tm element, it means Er and Tm doped alloy owns the more stable glassy state than that of Dy and Ho doped alloys. The crystallization behavior depends on the structural state of the glassy alloy, it may be the reason why Er and Tm containing alloys possesses an extra competitive Fe_3B crystallization phase. The competition of multiphase in Er- and Tm-containing alloys is beneficial for the stabilization of the liquid phases, which causes the better GFA. Meanwhile, the DSC traces show that these four alloys almost have the same SCLR, however as indicated by DIL measurements, their softness are different as a result of the distinction on the shear modulus G . Thus, Tm-containing alloy may be more suitable for thermoplastic machining among these four alloys due to the reason that it is relatively softer (smaller ΔG). On the other hand, with the increase of atomic number from Dy to Tm, σ_f shows decreasing trend because of the weak atomic bonding and the increase in flaw sensitivity and porosity, while the soft magnetic properties are significantly improved, which gives a better magnetic performance of the Tm-containing alloy, $\text{Fe}_{66}\text{Tm}_5\text{Nb}_6\text{B}_{23}$ that possesses an excellent GFA and magnetic properties, thereby, can be as a functional soft-magnetic material for the application of thermoplastic machining.

4. Conclusions

The influences of heavy RE addition on comprehensive properties of $\text{Fe}_{66}\text{RE}_5\text{Nb}_6\text{B}_{23}$ (RE = Dy, Ho, Er or Tm) glassy alloy system were investigated. The results are summarized below:

- (1) Doping 5 at. % heavy RE elements into $\text{Fe}_{71}\text{Nb}_6\text{B}_{23}$ glassy alloy effectively improves the GFA with D_c up to 4.5 mm. The SCLR and the crystallization process are varied by adding different heavy RE

Table 1

D_c , T_g , T_x , ΔT_x , B_s , H_c , σ_f and H_v of $\text{Fe}_{66}\text{RE}_5\text{Nb}_6\text{B}_{23}$ (RE = Dy, Ho, Er, and Tm) BMGs.

Alloy	D_c (mm)	Thermal stability			Magnetic properties		Mechanical properties	
		T_g (K)	T_x (K)	ΔT_x (K)	B_s (T)	H_c (A/m)	σ_f (GPa)	H_v (kg/mm ²)
$\text{Fe}_{66}\text{Dy}_5\text{Nb}_6\text{B}_{23}$	2	882 ± 2	972 ± 1	90 ± 3	0.46 ± 0.02	10.49 ± 0.12	3.65 ± 0.03	1060 ± 5
$\text{Fe}_{66}\text{Ho}_5\text{Nb}_6\text{B}_{23}$	3	883 ± 1	973 ± 2	90 ± 3	0.51 ± 0.03	11.28 ± 0.15	3.42 ± 0.05	1045 ± 5
$\text{Fe}_{66}\text{Er}_5\text{Nb}_6\text{B}_{23}$	4	882 ± 3	972 ± 1	90 ± 4	0.54 ± 0.02	8.78 ± 0.08	3.32 ± 0.07	1040 ± 5
$\text{Fe}_{66}\text{Tm}_5\text{Nb}_6\text{B}_{23}$	4.5	881 ± 2	971 ± 2	90 ± 4	0.58 ± 0.04	8.57 ± 0.14	3.15 ± 0.08	1020 ± 5

elements.

- (2) The GFA is affected by both atomic stacking and electronic structures. $\text{Fe}_{66}\text{RE}_5\text{Nb}_6\text{B}_{23}$ (RE = Er, Tm) owns three competitive formations of Fe_{23}B_6 , $\text{RE}_2\text{Fe}_{14}\text{B}$, and Fe_3B , much more complex than that of $\text{Fe}_{66}\text{RE}_5\text{Nb}_6\text{B}_{23}$ (RE = Ho, Dy), which contributes to the excellent GFA of $\text{Fe}_{66}\text{RE}_5\text{Nb}_6\text{B}_{23}$ (RE = Er, Tm). Besides, based on the XPS spectra, the $\text{Fe}_{66}\text{Tm}_5\text{Nb}_6\text{B}_{23}$ shows the lowest $N(E_F)$, which causes Tm doped alloy owns the most stable state with a shortened interatomic distance and the best GFA among these alloy systems.
- (3) Consistent with the observation in Zr-based BMG, a negative correlation between the $(\Delta L/L_0)_{s\text{-max}}$ and $\Delta G = G(\text{Fe}_{71}\text{Nb}_6\text{B}_{23}) - G(\text{RE})$ is found in $\text{Fe}_{66}\text{RE}_5\text{Nb}_6\text{B}_{23}$. $\text{Fe}_{66}\text{Tm}_5\text{Nb}_6\text{B}_{23}$ alloy owes the smallest ΔG corresponding to a good flowability in SCLR, which is more suitable for thermoplastic machining in the SCLR among these four alloys.
- (4) Although σ_f of Tm-containing sample decreases because of the weak atomic bonding and the increase in flaw sensitivity and porosity, the soft magnetic properties of $\text{Fe}_{66}\text{Tm}_5\text{Nb}_6\text{B}_{23}$ are significantly improved as compared to other RE-containing alloys due to the low magnetic moments of Tm and the weakened negative effect of B. Combined with the DIL measurement, it is expected that $\text{Fe}_{66}\text{Tm}_5\text{Nb}_6\text{B}_{23}$ with a good flowability and soft magnetic property can be as a potential functional materials.

Declaration of Competing Interest

The authors declared that they have no conflicts of interest to this work. We declare that we do not have any commercial or associative interest that represents a conflict of interest in connection with the work submitted.

Acknowledgements

This work was supported by the National Natural Science Foundation of China (Grant Nos. 51631003, 51601038, 51601130), the National Key Research and Development Program of China (Grant No. 2016YFB0300502), the Fundamental Research Funds for the Central Universities (Grant No. 2242019K40060).

References

- W.H. Wang, C. Dong, C.H. Shek, Bulk metallic glasses, *Mater. Sci. Eng. R* 44 (2004) 45–89.
- S.F. Guo, K.C. Chan, S.H. Xie, P. Yu, Y.J. Huang, H.J. Zhang, Novel centimeter-sized Fe-based bulk metallic glass with high corrosion resistance in simulated acid rain and seawater, *J. Non-Cryst. Solids* 369 (2013) 29–33.
- W.M. Yang, H.S. Liu, Y.C. Zhao, A. Inoue, K. Jiang, J.T. Huo, H.B. Ling, Q. Li, B.L. Shen, Mechanical properties and structural features of novel Fe-based bulk metallic glasses with unprecedented plasticity, *Sci. Rep.* 4 (2014) 6233.
- J.J. Si, C.X. Du, T. Wang, Y.D. Wu, R.S. Wang, X.D. Hui, Glass formation and soft magnetic properties of novel Fe-rich Fe-B-Ti-Zr bulk metallic glasses, *J. Alloys Compd.* 741 (2018) 542–548.
- J.H. Yao, J.Q. Wang, Y. Li, Ductile Fe-Nb-B bulk metallic glass with ultrahigh strength, *Appl. Phys. Lett.* 92 (2008) 251906.
- H.Y. Jung, S. Yi, Enhanced glass forming ability and soft magnetic properties through an optimum Nb addition to a Fe-C-Si-B-P bulk metallic glass, *Intermetallics* 18 (2010) 1936–1940.
- J.H. Yao, H. Yang, J. Zhang, J.Q. Wang, The influence of Nb and Zr on glass-formation ability in the ternary Fe-Nb-B and Fe-Zr-B and quaternary Fe-(Nb, Zr)-B alloy systems, *J. Mater. Res.* 23 (2008) 392–401.
- J.W. Li, W.M. Yang, M.X. Zhang, M.X. Zhang, G.X. Chen, B.L. Shen, Thermal stability and crystallization behavior of $(\text{Fe}_{0.75-x}\text{Dy}_x\text{B}_{0.2}\text{Si}_{0.05})_{96}\text{Nb}_4$ ($x = 0-0.07$) bulk metallic glasses, *J. Non-Cryst. Solids* 365 (2013) 42–46.
- F. Hu, Q. Luo, B.L. Shen, Thermal, magnetic and magnetocaloric properties of FeErNbB metallic glasses with high glass-forming ability, *J. Non-Cryst. Solids* 512 (2019) 184–188.
- F. Hu, C.C. Yuan, Q. Luo, W.M. Yang, B.L. Shen, Effects of Ho addition on thermal stability, thermoplastic deformation and magnetic properties of FeHoNbB bulk metallic glasses, *J. Alloys Compd.* 807 (2019) 151675.
- S.P. Pan, J.Y. Qin, T.K. Gu, The role of rare-earth elements in the structures of FeB-based glass forming liquid alloys, *J. Appl. Phys.* 107 (2010) 033503.
- H.J. Wang, G.J. Shiflet, S.J. Poon, K. Matsuda, S. Ikeno, The role of Y/lanthanides on the glass forming ability of amorphous steel, *Appl. Phys. Lett.* 91 (2007) 141910.
- M. Büttner, G.J. Shiflet, X.J. Gu, S.J. Poon, P. Reinke, Influence of erbium on the electronic structure of $\text{Fe}_{65-x}\text{Mo}_{14}\text{C}_{13}\text{B}_6\text{Er}_x$ ($x = 0, 1, 2$) bulk metallic glasses, *J. Appl. Phys.* 105 (2009) 023518.
- S.H. Sheng, C.L. Ma, S.J. Pang, T. Zhang, Glass-forming ability and mechanical properties of Sm-doped Fe-Cr-Mo-C-B glassy alloys, *Mater. Trans.* 46 (2005) 2949–2953.
- Q. Chang, C.L. Ma, S.J. Pang, H. Men, T. Zhang, Formation and mechanical properties of bulk glassy $(\text{Cu}_{0.55}\text{Zr}_{0.40}\text{Al}_{0.05})_{99}\text{RE}_1$ (RE = Y, Pr, Tb, Dy, Ho, Er) alloys, *Mater. Trans.* 47 (2006) 1257–1260.
- A. Takeuchi, A. Inoue, Classification of bulk metallic glasses by atomic size difference, heat of mixing and period of constituent elements and its application to characterization of the main alloying element, *Mater. Trans.* 46 (2005) 2817–2829.
- C.C. Yuan, F. Yang, X.K. Xi, C.L. Shi, D. Holland-Moritz, M.Z. Li, Hu, B.L. Shen, X.L. Wang, A. Meyer, W.H. Wang, Impact of hybridization on metallic-glass formation and design, *Mater. Today* (2019), <https://doi.org/10.1016/j.mattod.2019.06.in.press>.
- J.W. Li, D. Estévez, K.M. Jiang, W.M. Yang, Q.K. Man, C.T. Chang, X.M. Wang, Electronic-structure origin of the glass-forming ability and magnetic properties in Fe-RE-B-Nb bulk metallic glasses, *J. Alloys Compd.* 617 (2014) 332–336.
- Y. Lu, Y. Huang, J. Shen, The electronic structure origin for ultrahigh glass-forming ability of the FeCoCrMoCBy alloy system, *J. Appl. Phys.* 110 (2011) 033720.
- D. Cao, Y. Wu, X.J. Liu, H. Wang, X.Z. Wang, Z.P. Lu, Enhancement of glass-forming ability and plasticity via alloying the elements having positive heat of mixing with Cu in $\text{Cu}_{48}\text{Zr}_{48}\text{Al}_4$ bulk metallic glass, *J. Alloys Compd.* 777 (2019) 382–391.
- Y.R. Zhang, R.V. Ramanujan, The effect of niobium alloying additions on the crystallization of a Fe-S-B-Nb alloy, *J. Alloys Compd.* 403 (2005) 197–205.
- J. Fornell, S. González, E. Rossinyol, S. Suriñach, M.D. Baró, D.V. Louzguine-Luzgin, J.H. Perepezko, J. Sort, A. Inoue, Enhanced mechanical properties due to structural changes induced by devitrification in Fe-co-B-Si-Nb bulk metallic glass, *Acta Mater.* 58 (2010) 6256–6266.
- S.T. Nagel, J. Tauc, Nearly-free-electron approach to the theory of metallic glass alloys, *Phys. Rev. Lett.* 35 (1975) 380–383.
- S.F. Guo, C. Su, J.X. Cui, J. Li, G.N. Li, M. Zhang, N. Li, Effects of B addition on glass forming ability and thermal behavior of FePC-based bulk metallic glasses, *J. Iron Steel Res. Int.* 24 (2017) 442–447.
- Q. Hu, M.W. Fu, X.R. Zeng, Thermostability and thermoplastic formability of $(\text{Zr}_{65}\text{Cu}_{17.5}\text{Ni}_{10}\text{Al}_{7.5})_{100-x}\text{RE}_x$ ($x = 0.25-3.25$, RE: Y, Gd, Tb, Dy, Ho, Er, Tm, Yb, Lu) bulk metallic glasses, *Mater. Design* 64 (2014) 301–306.
- M.D. Demetriou, W.L. Johnson, K. Samwer, Rheology and ultrasonic properties of metallic glass-forming liquids, *J. Alloys Compd.* 483 (2009) 650–654.
- J.M. Park, G. Wang, R. Li, N. Mattern, J. Eckert, D.H. Kim, Enhancement of plastic deformability in Fe-Ni-Nb-B bulk glassy alloys by controlling the Ni-to-Fe concentration ratio, *Appl. Phys. Lett.* 96 (2010) 031905.
- The Periodic Table, Available at, 2019. <http://periodictable.com/>.
- J.W. Li, A.N. He, B.L. Shen, Effect of Tb addition on the thermal stability, glass-forming ability and magnetic properties of Fe-B-Si-Nb bulk metallic glass, *J. Alloys Compd.* 586 (2014) S46–S49.
- C.C. Yuan, C. Deng, H.P. Zhang, M.Z. Li, B.L. Shen, Ab initio simulations of the atomic and electronic environment around B in Fe-Nb-B metallic glasses, *Intermetallics* 112 (2019) 106501.
- E. Lopatina, I. Soldatov, V. Budinsky, M. Marsilius, L. Schultz, G. Herzer, R. Schäfer, Surface crystallization and magnetic properties of $\text{Fe}_{84.3}\text{Cu}_{0.7}\text{Si}_4\text{B}_8\text{P}_3$ soft magnetic ribbons, *Acta Mater.* 96 (2015) 10–17.
- J.W. Li, H. Men, B.L. Shen, Soft-ferromagnetic bulk glassy alloys with large magnetostriction and high glass-forming ability, *AIP Adv.* 1 (2011) 042110.
- M. Kersten, *Problem der Technischen Magnetisierungs Kurve*, Springer, Berlin, 1938, p. 42.
- C.C. Yuan, J.F. Xiang, X.K. Xi, W.H. Wang, NMR signature of evolution of ductile-to-brittle transition in bulk metallic glasses, *Phys. Rev. Lett.* 107 (2011) 236403.
- C.C. Yuan, X. Shen, J. Cui, L. Gu, R.C. Yu, X.K. Xi, Atomic and electronic structures of Zr-(Co,Ni,Cu)-Al metallic glasses, *Appl. Phys. Lett.* 101 (2012) 021902.
- Z.Q. Liu, Z.F. Zhang, Mechanical properties of structural amorphous steels: intrinsic correlations, conflicts, and optimizing strategies, *J. Appl. Phys.* 114 (2013) 243519.
- J.W. Li, W.M. Yang, D. Estévez, G.X. Chen, W.G. Zhao, Q.K. Man, Y.Y. Zhao, Z.D. Zhang, B.L. Shen, Thermal stability, magnetic and mechanical properties of Fe-Dy-B-Nb bulk metallic glasses with high glass-forming ability, *Intermetallics* 46 (2014) 85–90.